Siberian Branch of Russian Academy of Science
BUDKER INSTITUTE OF NUCLEAR PHYSICS

A. Aulchenko, O. Evdokov, P. Papushev,
S. Ponomarev, L. Shekhtman, K. Ten,
B. Tolochko, I. Zhogin, V. Zhulanov

ONE-DIMENSIONAL DETECTOR WITH 100-ns RESOLUTION FOR STUDY OF EXPLOSIONS USING SYNCHROTRON RADIATION

Budker INP 2002-55

Novosibirsk
2002

One-dimensional detector with 100-ns resolution for study of explosions using synchrotron radiation

A. Aulchenko[a], *O. Evdokov*[b], *P. Papushev*[a], *S. Ponomarev*[a], *L. Shekhtman*[a,1], *K. Ten*[c], *B. Tolochko*[b], *I. Zhogin*[b], *V. Zhulanov*[a]

[a] Budker Institute of Nuclear Physics, 630090 Novosibirsk, Russian Federation

[b] Institute of Solid State Chemistry and Mechano-Chemistry, 630090 Novosibirsk, Russian Federation

[c] Lavrentiev Institute of Hydrodynamics, 630090 Novosibirsk, Russian Federation

Abstract

Investigation of fast dynamic processes with the help of synchrotron radiation allows to understand properties of short life-time states of materials at very high temperatures and pressures. Detector for such studies has to be able to detect X-ray photons from each electron bunch separately with position resolution of about 0.1 mm. The prototype of the detector for imaging of explosions at SR beam (DIMEX) is described in the paper. Spatial resolution of ~ 300 μ and time resolution of $\sim$ 100 ns is demonstrated with SR beam from VEPP-3 2T wiggler and electron beam energy of 2 GeV. Results of the first projective imaging and SAXS experiments are presented.

key words: Synchrotron radiation, Imaging, detectors, explosions, time resolution

[1] Corresponding author. Address: Budker Institute of Nuclear Physics, 11 Lavrentiev Avenue, Novosibirsk 630090, Russia. Tel: 7(3832)394992, Fax: 7(3832)342163, e-mail: L.I.Shekhtman@inp.nsk.su

Preprint submitted to Elsevier Preprint

1 Introduction

Synchrotron radiation was shown to be a powerful tool to study very fast physical and chemical processes appearing at high temperatures and pressures during explosions [1, 2]. Very short pulses of synchrotron light irradiated by individual electron bunches allow imaging of the development of detonation wave as well as fluctuations of electron density within the volume of the exploding materials. Such experiments require exceptional set of parameters from the detector. In order to view images from different electron bunches independently, time resolution of the detector has to be less than bunch crossing time. For VEPP-3 storage ring this time equals 250 ns in a single bunch mode. Spatial resolution of ~ 0.1 mm allows viewing of shock wave structure in projective imaging experiments. Efficiency of more than 50% is very desirable in order to get good photon statistics. Finally, an efficient imaging at such frame rate requires very high rate capability of $10^{10} - 10^{11}\,\mathrm{photons{\cdot}s^{-1}{\cdot}mm^{-2}}$. At such photon rate the detector can work only in charge integrating mode. Another restriction comes from the requirement of high frame rate. Storage of a frame within ~ 100 ns is quite difficult. Thus, raw data from the detector have to be stored in analogue form during the experiment. After the end of the measurement data can be slower digitized and stored in a final storage medium.

One of the possible schemes for such detector is shown in Fig.1. Microstrip structure is used to detect charge from direct conversions of photons in sensitive material. Coupled to the strips are integrators with fast analogue memory where detected charge can be stored quickly after the end of each frame. Whole analogue memory can be readout, digitized and stored in an external buffer after the end of full series.

We considered as possible materials for the detector Si, GaAs and pressurized Xe. Comparison of absorption efficiency for these 3 materials is shown in Fig.2. Si has quite low efficiency at the energies higher than 15 keV. GaAs is heavier material and its absorption efficiency is rather high. However its hole mobility of $\sim 400\,\mathrm{cm^2 \cdot V^{-1}{\cdot}s^{-1}}$ is much lower than the electron one ($\sim 10000\,\mathrm{cm^2 \cdot V^{-1}{\cdot}s^{-1}}$) and can be not enough for collection of full charge

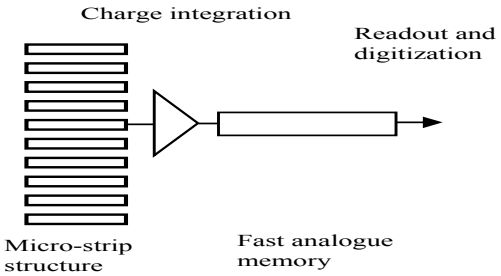

Figure 1: Possible scheme of fast detector for imaging of SR light from individual bunches.

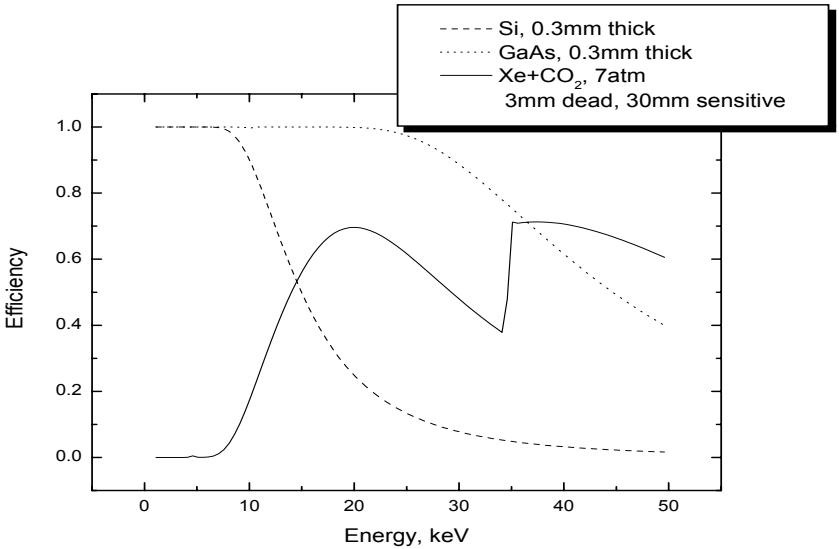

Figure 2: Comparison of the absorption efficiency of micro-strip detector with 3 different sensitive materials: Si, 0.3 mm thick; GaAs, 0.3 mm thick; Xe, 7 atm, 3 mm dead zone and 30 mm sensitive region.

within ~ 100 ns. Ion mobility of Xe is very low, about $0.53\,\mathrm{cm}^2 \cdot V^{-1} \cdot \mathrm{s}^{-1}$ [3]. However ions can be shielded in gas detector with metal grid. High electron drift velocity in mixtures of $Xe{-}CO_2$ with amount of CO_2 more than 10% allows to collect charge well within ~ 100 ns.

In the present paper we introduce a new detector for imaging of fast dynamic processes and explosions with SR beam (DIMEX). The detector is based on ionization chamber with charge collection to a microstrip structure coupled to ASIC with integrators and fast analogue memory.

2 Detector design

DIMEX consists of a micro-strip structure with 100μ pitch, put in the gas volume filled with $Xe{-}CO_2$ $(80 - 20\%)$ at 7 atm, and high voltage drift electrode pushing electron component of the primary ionization to the readout strips (Fig.3). Shielding of the ionic component of primary ionization is performed by Gas Electron Multiplier (GEM) [4], stretched at a distance of 1 mm above the micro-strip structure. The distance between drift electrode and GEM foil is 2 mm.

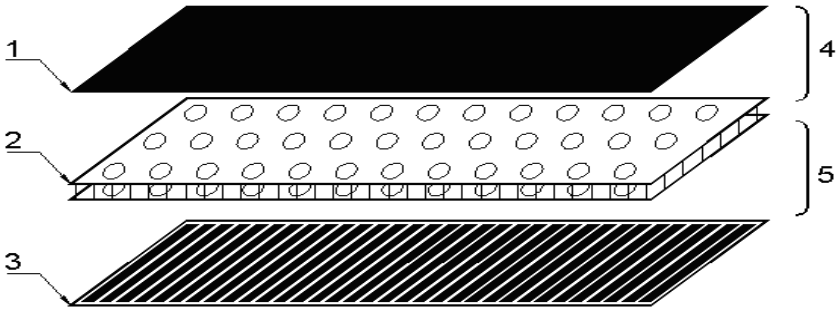

Figure 3: Schematic design of the sensitive part of DIMEX. 1 - drift electrode; 2 - GEM; 3 - micro-strip structure; 4 - conversion gap; 5 - induction gap.

Narrow beam of SR (~ 1 mm high) either after absorption in an object or after scattering gets into the conversion volume between the drift electrode and GEM. Electronic component of primary ionization drifts towards GEM, penetrates through it and then induces charge at the strips. Ions drift towards the drift electrode and do not induce any charge to the readout strips. GEM is a micro-structure consisting of regularly punched holes in an insulating

(kapton) foil, double clad with thin copper layers. Foil thickness is 50μ, holes pitch is 140μ and holes diameter is $\sim 80\mu$. By choosing appropriate voltage between the metal layers on GEM sides we can flexibly tune the fraction of charge penetrating through the foil or amplify it.

Readout strips are connected to the input pads of APC128 ASIC [5]. The ASIC consists of 128 channels with low-noise integrators at the input and 32-cell analogue pipe-line. All 128 pipe-lines can be readout in series through analogue multiplexer (Fig.4).

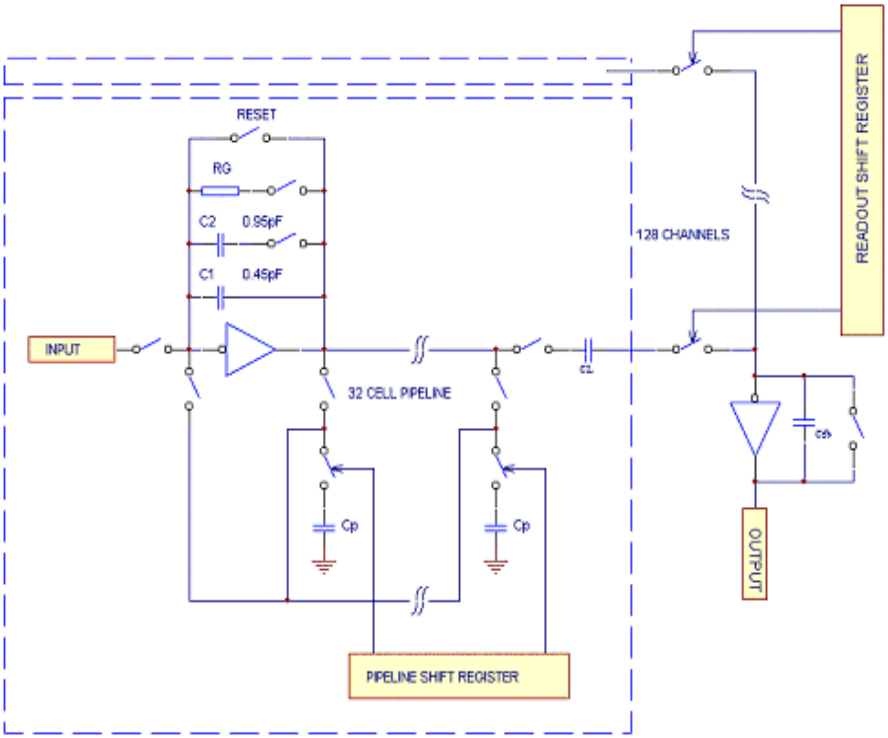

Figure 4: Schematics of the APC128 ASIC.

Detector operation includes several stages. The external start signal initiates the measurement sequence, when the pipe-line cells are coupled in series to the output of integrators synchronously with the clock pulses. Clock frequency can be different depending on particular regime. In such a way the frames of an experimental sequence are formed. After the filling of all 32 pipe-

line cells the measurement sequence is stopped and the read-out sequence is initiated. During the read-out sequence each pipe-line cell is connected to the input of the integrator with previously reset feedback capacitor. The output of the integrators is readout through the output multiplexer. As the input integrator is used twice, during the measurement sequence and during the readout sequence, the output signal is reversely proportional to the square of the feedback capacitor. The sensitivity and, thus, the dynamic range of the ASIC can be changed by connecting additional feedback capacitor to the integrator. Reduction of the sensitivity in this case can widen the dynamic range by 3.1 and 9.7 times (C2 capacitor can be connected only for the measurement or for all the time). Parameters of different regimes are listed in Table 1.

Table 1: Parameters of different regimes for APC128 operation

Feedback capacitor	C1	C1+C2 measurement, C1 readout	C1+C2
Noise equivalent charge (electrons)	1270	1490	1910
Maximum signal(electrons)	$0.25 \cdot 10^6$	$0.72 \cdot 10^6$	$2.3 \cdot 10^6$
Maximum signal to noise ratio	190	480	790

During the measurement sequence APC128 can operate either with the reset between individual measurements or without it.

Each of the described regimes can be chosen flexibly for the optimization of a particular experiment. The block-diagram of detector electronics is shown in Fig.5.

Electronics is assembled in the gas volume. In case of DIMEX prototype it includes 2 APC128 chips, 2 14-bit ADC, 256-Kbyte RAM and PLD ALTERA EPF10K20, that controls all the elements and provides connectivity with the network module IP302 outside the hermetic case (Fig.6).

3 Experimental set-up and results

For the study of main detector parameters such as spatial and time resolution, and signal-to-noise ratio we used several set-ups. Main set-up that was also used for the experiments with explosions is shown schematically in Fig.7. It uses white SR beam from 2T wiggler at VEPP-3 storage ring. The set-up consists of 3 chambers. The first chamber contains collimators that form the necessary beam shape. The second one is the explosion chamber where

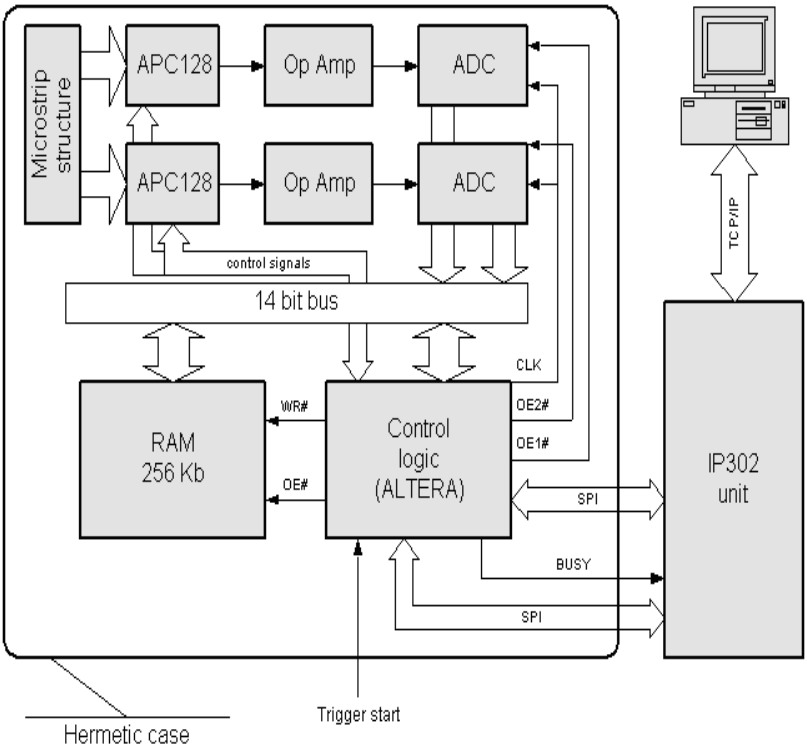

Figure 5: Block-diagram of the detector electronics.

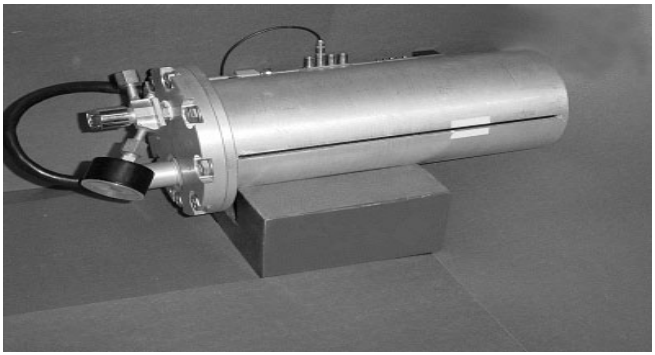

Figure 6: Outside view of the DIMEX prototype.

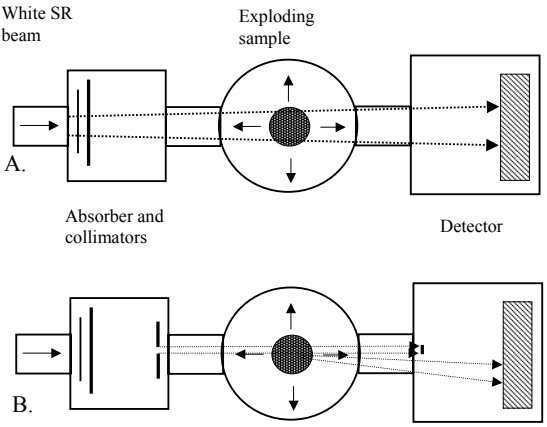

Figure 7: Schematics of the set-up for the experiments with exploding sample. A - set-up for the projective absorption experiments; B - set-up for SAXS experiments. The sample-detector distance L=1050 mm.

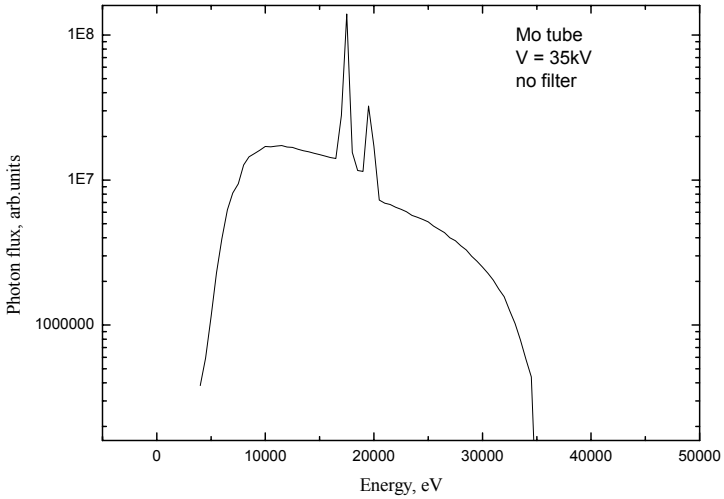

Figure 8: Energy spectrum of the X-ray tube with Mo anode. Tube voltage is 35 kV.

the sample is exploded. It has beryllium windows with shock wave reducers that protect the beam line from the detonation wave. The third chamber contains the detector with the second collimator and additional shutter for SAXS experiments.

Some measurements have been performed with X-ray tube with Mo anode. Spectra from X-ray tube and 2T wiggler used for the measurements are shown in Fig.8 and Fig.9.

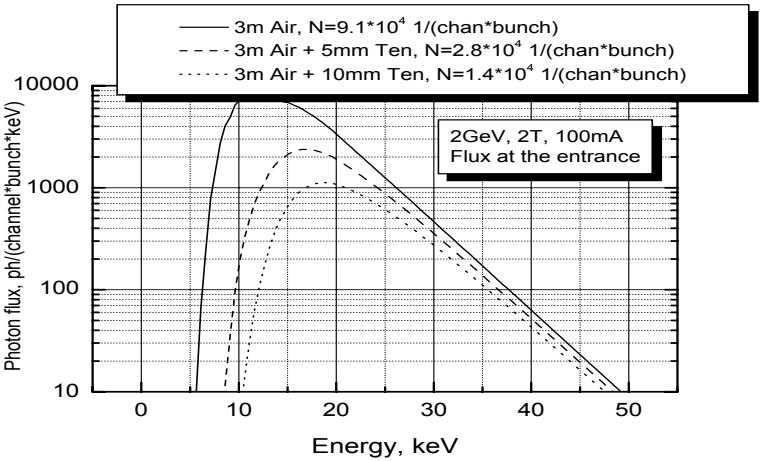

Figure 9: Energy spectrum of the beam from 2T wiggler.Spectra before and after 5mm and 10mm explosive(TEN) are shown. Total flux (integral over the whole energy range) is indicated as N.

3.1 Spatial resolution

Spatial resolution of DIMEX is determined by secondary particles, namely photo-electrons, fluorescent photons and Auger-electrons emitted after photo-conversion in Xe. As the energy is below Xe K-edge ($\sim$ 35 keV) Auger-electrons and fluorescent photons have low energy (below 5 keV), and spatial resolution is mainly affected by energetic photo-electrons. Passage of the electrons with the energy in the range of tens keV can not be calculated analytically and we used GEANT4 simulation package [6] to estimate the detector resolution for several experimental conditions. In Fig.10 the line spread function (detector response for very narrow beam) for 3 different gas pressures is shown. Simulation was performed for the photons from X-ray tube with Mo target at 35 keV.

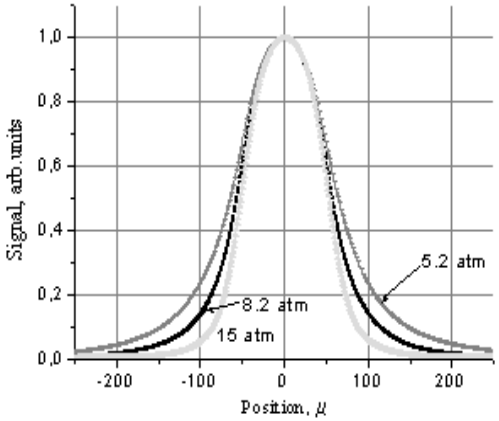

Figure 10: Line spread function for 3 different pressures of Xe, simulated with GEANT4. X-rays from Mo tube at 35 keV.

From the figure one can see that the resolution is affected by pressure and improves from $\sim 140\mu$ to $\sim 110\mu$ (FWHM), when pressure is increased from 5 to 15 atm.

However the result of the measurement with X-ray tube beam (Fig.11) is worse than the simulation, indicating that GEANT4 is not yet well tuned. From the figure we can see that experimental resolution at 7 atm is $\sim 300\mu$ (FWHM) and more than twice worse than the result of simulation.

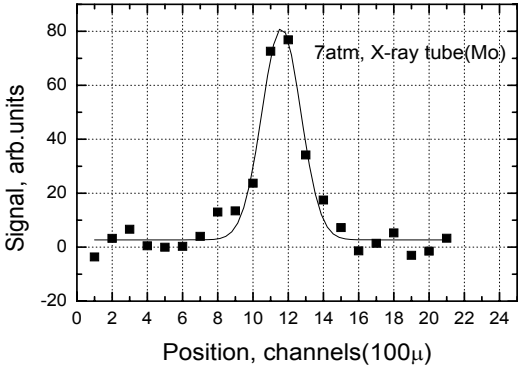

Figure 11: Line spread function measured for the beam from Mo tube at 35 keV. Detector is at 7 atm.

Spatial resolution (line spread function) for the main experimental conditions with the beam from the wiggler is shown in Fig.12. It is very similar to the result with X-ray tube, as main part of the spectrum of SR beam has its energy around 20 keV.

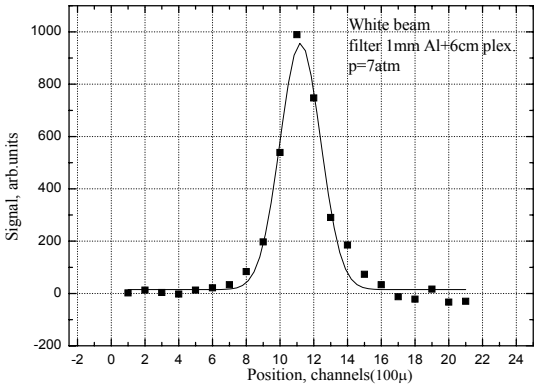

Figure 12: Line spread function measured for the beam from 2T wiggler. Detector is at 7 atm.

3.2 Time resolution

The most critical parameter of the detector is time resolution. In order to have really independent images from individual electron bunches, time resolution has to be better than bunch crossing time. For VEPP-3 this time is equal to 250 ns in single bunch mode. Time resolution is determined by the electron drift velocity, beam height and the accuracy of the distance from the beam plane to the GEM plane. Longitudinal diffusion of electrons also slightly affects the resolution.

In order to measure time resolution the detector was operated at 125 ns clock period, that is equal to half bunch crossing time. In this case the detector is irradiated only within one out of two successive clock periods. With such short clock period DIMEX can be operated only in the regime without the reset, as the latter can not be fast and needs ~ 150 ns. Thus in an ideal case the dependence of the signal versus time must look as "steps" with the width of 2 clock periods. The difference with this picture gives information about the real time resolution. An example of such measurement is shown in Fig.13.

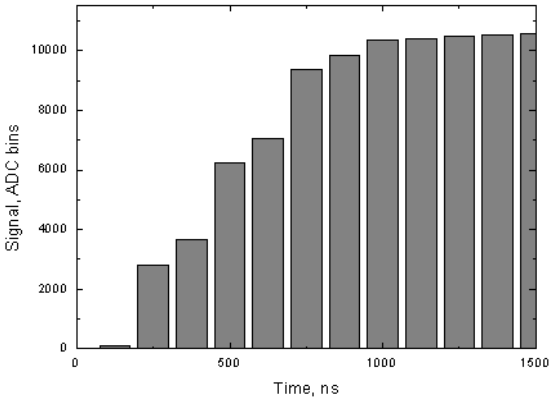

Figure 13: Dependence of signal in one of the detector channels versus time. Clock period is 125 ns, no reset.

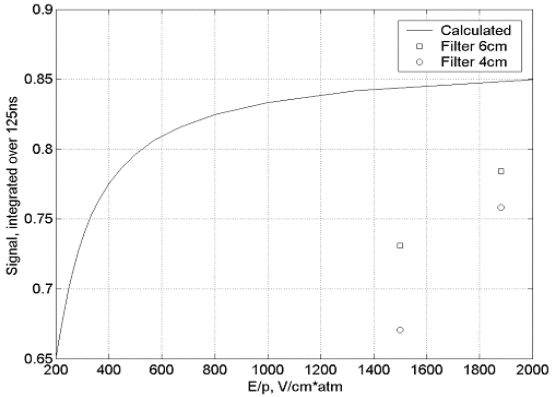

Figure 14: Fraction of charge collected within 125 ns after the bunch crossing as a function of reduced electric field. Experimental results correspond to different photon fluxes: 540 ph/chan (4cm plex.filter) and 220 ph/chan (6cm plex.filter).

The dependence of fraction of charge collected within 125 ns after the bunch crossing as a function of reduced electric field is shown in Fig.14 for four different conditions of measurements. Open squares and open circles correspond to a different photon flux, 540 ph/chan and 220 ph/chan. As we will see below, at higher rates space charge effects cause some field distortion that can affect charge collection time. In Fig.14 the result of calculation is also plotted. The calculation has taken into account the thickness of the beam of 1mm, electrons drift time in the gap below GEM and time constant of the integrator.

From the comparison of experimental result with the calculation we see that there is significant factor that worsen charge collection time. Most probably this is misalignment of the detector with respect to the beam and more studies needed to understand this effect. However even at this stage we can state that at the field higher than 1.8 kV/cm·atm the fraction of charge collected within 125 ns is more than 0.75. Assuming exponential dependence of the signal versus time we get that within 250 ns the fraction collected is equal to 0.95.

3.3 Signal, noise, efficiency

The accuracy of signal measurements is determined by a fraction of primary beam absorbed by the detector (efficiency), saturation and other distortions of the signal, noise value. We can distinguish the following noise components: electronic noise (noise without any irradiation), statistical fluctuations due to limited number of photons detected (quantum noise) and fluctuations of signal from individual photon.

In Fig.15 the calculated efficiency as function of energy is shown for several values of the dead zone before the sensitive region for 7 atm $Xe-CO_2$ $(80-20\%)$ mixture. The sensitive region is 30 mm long. In the prototype the dead zone is 3mm long and efficiency is close to 60% in the energy range around 20 keV.

Using the X-ray tube, calibrated with 100% efficient counting detector based on CdTe crystal, the linearity of the DIMEX response was measured. The measurement was performed in a very slow mode with exposure time of 3.2ms because of low flux as compared to SR beam. The results are shown in Fig.16. In spite of so long exposure the whole dynamic range could not be covered. We can see that in the combined regime, when the measurement is done with high feedback capacitance and the readout is performed with low feedback capacitance, the highest signal reached is $\sim$ 3000 ADC bins while the saturation of the integrator occurs at $\sim$ 10000 ADC counts. The

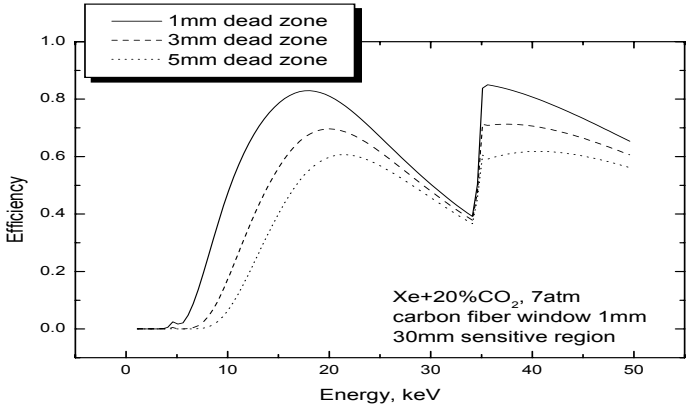

Figure 15: Efficiency as a function of energy for a different lengths of the dead zone before the sensitive region. Gas pressure is equal to 7 atm.

linearity is very good in the measured range for two regimes with combined feedback capacitance and with high feedback capacitance. The regime with low feedback capacitance and the highest sensitivity could not be realized at such long exposures. From these results the signal from one photon can be calculated assuming a certain value of efficiency (we took 0.6).

The results of calculation of the conversion factor (signal per one photon), maximum number of photons before saturation of the integrator and the dynamic range are shown in Table 2. The value of dynamic range here is calculated as the ratio of maximum number of photons before saturation and statistical fluctuation of this number (i.e. square root), assuming that other noise sources are low at the maximum signal.

Table 2: Some parameters of the detector in terms of 20 keV photons at different values of integrator feedback capacitor. Electronic noise is shown in brackets in the first row.

Feedback capacitor	C1	C1+C2 measurement, C1 readout	C1+C2
Signal per 20 keV photon, ADC bins	50 (83)	15.5(16)	4.8 (9)
Maximum signal, 20 keV photons	200	645	2083
Dynamic range	14	25	46

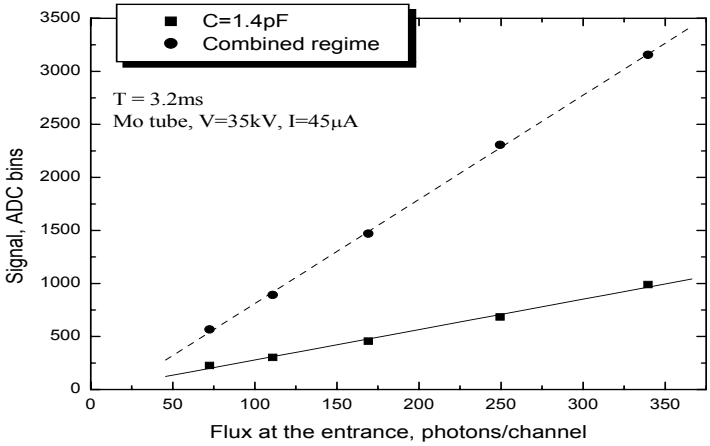

Figure 16: Signal as a function of X-ray flux per channel at the entrance window the detector. Results are shown for the regime with high feedback capacitance and combined regime (high capacitance during the measurement and low capacitance during the readout.

However at the real experimental conditions saturation of the signal occurs earlier than at $\sim$ 10000 ADC bins, as one can see in Fig.17. Here the results of the measurements in two regimes are shown, with low feedback capacitance and with high feedback capacitance. The clock period was 500 ns (frame size) and the second bunch in the frame was masked by the reset signal. The saturation of signal in both regimes occurs at approximately the same photon flux of $\sim$ 400 photons per channel. This value is strongly affected by the electric field, that indicates the space charge nature of the effect. Slow ions are accumulated in the conversion gap and distort the field such that electrons can not be effectively transported.

One of the convenient parameters for characterization of the precision of signal measurement is signal-to-noise ratio. For the counting detector without intrinsic noise the value of signal-to-noise ratio is in simple relation with the efficiency and input flux $(S/n)^2 = \varepsilon \cdot N_i n$. Square of the signal-to-noise ratio is called Noise Equivalent Quanta (NEQ), as this is the number of photons that makes statistical fluctuations equal to the total noise of the detector. NEQ as a function of input flux for the same two regimes as in Figure 17, is shown in Fig.18.

NEQ for the case of 100% efficient counting detector is shown in the figure as dashed line. The ratio of the NEQ for particular case and the one for the

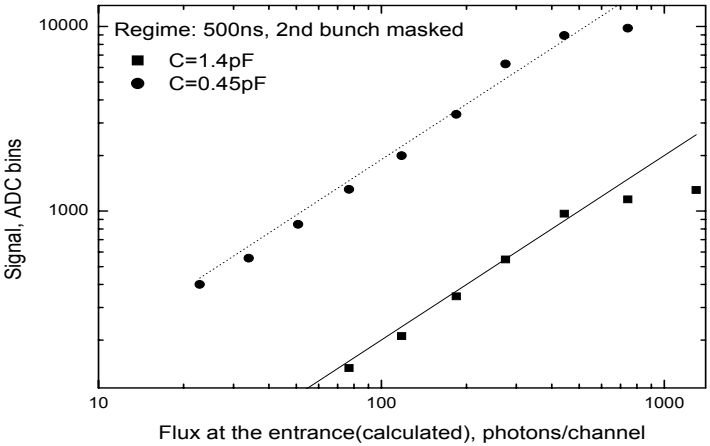

Figure 17: Signal as a function of X-ray flux per channel at the entrance window the detector for the real experimental conditions. Results are shown for the regimes with high feedback capacitance and low feedback capacitance.

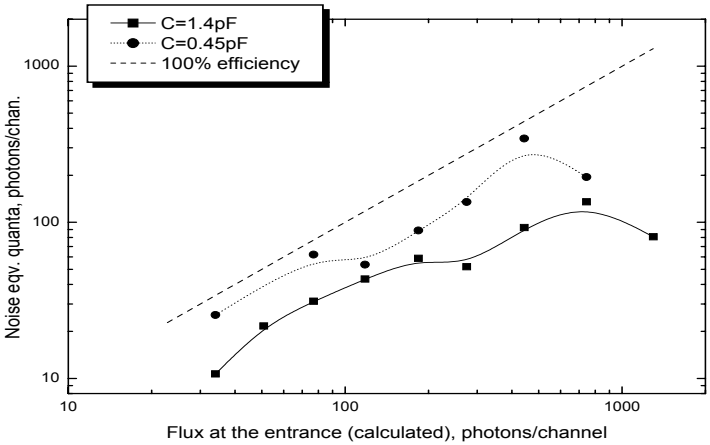

Figure 18: NEQ as a function of input flux. Results are shown for the regimes with high feedback capacitance and low feedback capacitance.

ideal detector gives the value of Detective Quantum Efficiency (DQE). For the regime with low feedback capacitance DQE is equal to $\sim 50\%$, while for the regime with high feedback capacitance DQE is much lower. This can only happen due to some additional electronic noise appearing during the measurement in real experimental conditions. This additional noise source will be investigated during further studies.

3.4 Results of the experiments

Two main types of experiments were performed using DIMEX. In order to investigate the structure and velocity of detonation wave in an explosive, as well as density distribution inside and around the exploding sample, the projective absorption experiments were realized. In these experiments the collimated line-shaped beam passes through the sample and the distribution of X-ray flux after the sample is measured with the detector. In our case the beam was $\sim$ 12 mm wide and 1mm high. The samples were 12.5 mm diameter and $\sim$ 100 mm long cylinders made of mixture of hexagene and TNT $(50 - 50\%)$. The sample was positioned with its axis either parallel to the beam plane, or perpendicular to it. The starting moment of the measurement sequence could be synchronized with the detonation within $\sim 0.5\mu$s.

The result of a series of projective absorption experiments is shown in Fig.19. In order to improve the precision, the results of 10 measurements were summed with proper synchronization. Horizontal axis of the figure is position perpendicular to the axis of the sample. Time axis is in vertical in units of 500 ns. The figure clearly shows the front of detonation wave, structure of the reaction zone and the flow of explosion products.

Small angle scattering (SAXS) experiments allow investigation of electron density distribution in an object. The evolution of SAXS image gives information about the density and size distributions of particles in an object. The example of SAXS experiment with explosion is shown in Fig.20. X-axis is position in detector channels, Y-axis is time in units of 250 ns. There is clear maximum that appears at $\sim 1\mu$s after the detonation. We believe that it indicates the process of diamonds formation out of free carbon in the explosion products.

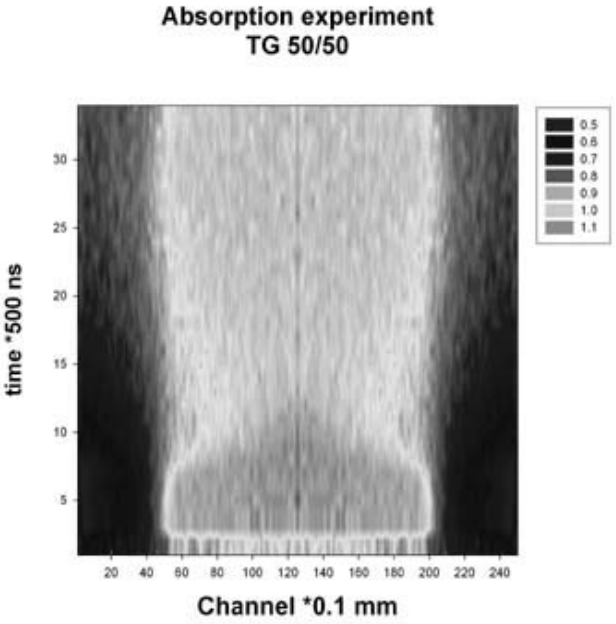

Figure 19: Result of the series of projective absorption experiments (10 explosions). Horizontal axis - position in channels ($100\,\mu$), vertical axis - time in units of 500 ns.

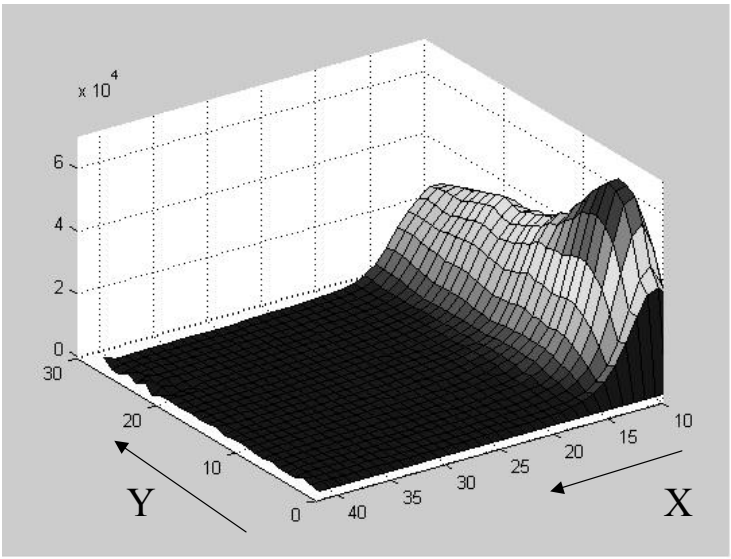

Figure 20: Result of the series of SAXS experiments (10 explosions). X-axis is angle in units of 10^{-4}, Y-axis is time in units of 250 ns.

3.5 Discussion and conclusions

In the present work we have demonstrated, that the concept of a very fast detector for the imaging, using SR flashes from individual bunches, can be realized. The first prototype of DIMEX has shown spatial resolution of $\sim 300\,\mu$ (FWHM), time resolution of ~ 100 ns and dynamic range of ~ 15. Maximum photon rate before saturation has been ~ 200 photons per channel per bunch. This value corresponds to photon flux of $\sim 10^{10}\,\mathrm{mm}^{-2}\cdot\mathrm{s}^{-1}$. The dynamic range and maximum photon flux are limited by space charge effect and additional electronic noise produced during operation of APC128 chip in a regime with high frame rate. Solution of these problems can allow improvement of dynamic range up to ~ 50 and maximum photon rate up to ~ 2000. These values are determined only by APC128 properties and further improvements will be possible only through development of a new ASIC.

Even with the present moderate dynamic range the first experiments with exploding samples have shown great potential of the techniques. By performing several experiments with identical conditions and synchronization we could improve accuracy adding the results together. Projective absorption experiments have shown the ability of the method to improve significantly

the information needed for the precise hydrodynamic model of explosion and to provide new knowledge about the structure of reaction zone. For the first time SAXS experiments have been performed with such object, demonstrating that we can really get information about the electron density fluctuations of exploding material. The technique of very fast imaging opens an opportunities in an area of fast dynamic small-angle X-ray scattering and wide-angle X-ray scattering (WAXS) studies of an objects under the influence of either different external factors like temperature, pressure, light etc., or internal meta-stable states. We believe that this will start a breakthrough in the research and development in the fields of material science that were not available for studies before.

Acknowledgements. Authors would like to thank very much Roland Horisberger, who provided APC128 ASICs and all relevant information.

References

[1] *A.N.Aleshaev el.al.* Nucl. Instr. and Meth. A470 (2001), 240.

[2] *B.P.Tolochko et.al.* Nucl. Instr. and Meth. A467-468 (2001), 990.

[3] *A.A.Radtzig, B.M.Smirnov.* In: Plazma Chemistry, issue 11, p.170, Energoizadat, Moscow, 1984.

[4] *F.Sauli.* Nucl. Instr. and Meth. A386 (1997) 531.

[5] *R.Horisberger, D.Pitzl.* Nucl. Instr. and Meth. A326(1993) 92.

[6] *S.Agostinelli et al.* "A Simulation toolkit, GEANT4", CERN-IT-2002-003, KEK-2002-85, SLAC-PUB-9350, Aug 2002, 86 pp. Accepted for publication in NIMA.

A. Aulchenko, O. Evdokov, P. Papushev,
S. Ponomarev, L. Shekhtman, K. Ten,
B. Tolochko, I. Zhogin, V. Zhulanov

One-dimensional detector
with 100-ns resolution for study of explosions
using synchrotron radiation

А. Аульченко, О. Евдоков, П. Папушев
С. Пономарев, Л. Шехтман, К. Тен,
Б. Толочко, И. Жогин, В. Жуланов

Однокоординатный детектор
со 100-наносекундным разрешением
для изучения взрывных процессов
с использованием синхротронного излучения

Budker INP 2002-55

Ответственный за выпуск А.М. Кудрявцев
Работа поступила 1.10.2002 г.

Сдано в набор 2.10.2002 г.
Подписано в печать 3.10.2002 г.
Формат бумаги 60×90 1/16 Объем 1.5 печ.л., 1.2 уч.-изд.л.
Тираж 170 экз. Бесплатно. Заказ № 55

Обработано на IBM PC и отпечатано на
ротапринте ИЯФ им. Г.И. Будкера СО РАН
Новосибирск, 630090, пр. академика Лаврентьева, 11.